

Interacting multiwave mixing in a five-level atomic system

Zhiqiang Nie,¹ Huaibin Zheng,¹ Peizhe Li,¹ Yongming Yang,¹ Yanpeng Zhang,^{1,2,*} and Min Xiao²

¹Key Laboratory for Physical Electronics and Devices of the Ministry of Education, Xi'an Jiaotong University, Xi'an 710049, China

²Department of Physics, University of Arkansas, Fayetteville, Arkansas 72701, USA

(Received 6 January 2008; revised manuscript received 21 March 2008; published 20 June 2008)

We study three (nested, parallel, and sequential cascade) types of schemes for doubly dressed four-wave-mixing processes in an open five-level atomic system. The interaction between two dressing fields of the nested-cascade scheme is strongest and weakest for the parallel-cascade scheme, with the sequential scheme intermediate between them. Mutual-dressing processes and constructive or destructive interference between two coexisting dressed multiwave mixing channels in such a system are also considered. Investigations of these multidressing mechanisms and interactions are very useful to understand and control the generated high-order nonlinear optical signals.

DOI: [10.1103/PhysRevA.77.063829](https://doi.org/10.1103/PhysRevA.77.063829)

PACS number(s): 42.50.Gy

I. INTRODUCTION

Many studies of high-order multiwave-mixing (MWM) processes have been carried out in the past few decades [1–9]. Enhanced four-wave-mixing (FWM) processes due to atomic coherence have been experimentally demonstrated in four-level systems including N-type and double- Λ -type atomic systems [1–4]. Also efficient six-wave mixing (SWM) has been observed in a four-level close-cycled N-type rubidium atomic system [5]. Moreover, eight-wave mixing (EWM) in a folded five-level atomic system has been experimentally demonstrated recently [6]. In the previously studied close-cycled (ladder-type, N-type, double- Λ -type, and folded) systems, the FWM, SWM, and EWM processes cannot coexist in a given configuration and different order nonlinearities can only be observed individually. In our recent studies, we demonstrated that the third-order and fifth-order nonlinear processes can coexist in the open (such as V-type, Y-type, and inverted Y-type) atomic systems. The coexisting SWM processes can become comparable or even greater in amplitude than the companion FWM processes by manipulating the atomic coherence and multiphoton interferences between different energy levels in the systems [7–9]. Different from those previous works, here we present our study of an open five-level system [Fig. 1(a)], in which the FWM, SWM, and EWM processes can all coexist under certain conditions.

Investigations on the interactions of doubly dressed states and the corresponding effects of atomic systems have attracted many researchers in recent years [10–16]. The interaction of double-dark states (nested-cascade scheme of doubly dressing) and splitting of a dark state (the secondarily dressed states) in a four-level atomic system were studied theoretically in an electromagnetically induced transparency (EIT) system by Lukin *et al.* [10]. Later, the triple-peak absorption spectrum, which was observed in the N-type cold-atomic system by Zhu *et al.*, verified the existence of the secondarily dressed states in the nested-cascade scheme [11]. A similar result was obtained in the inverted-Y system

[12,13]. After that, the doubly dressed FWM (DDFWM) in the nested-cascade, close-cycled atomic system was reported [15]. After that, two kinds of DDFWM processes (in parallel- and nested-cascade schemes) were considered in an open five-level atomic system [16]. In this work, we present three kinds of doubly dressing schemes for DDFWM and show similarities and differences among these different dressing schemes.

Recently, we have experimentally studied mutual dressing processes that existed between two competing, dressed FWM processes in a four-level Y-type atomic system [17]. Such dressing fields perturb both FWM processes and modify the total signal amplitude when these two FWM signals are tuned together in frequency. Constructive or destructive interference, which is a result of variation of phase difference between the two dressed FWM processes (also considered in two-level and three-level atomic systems as the coupling-field detuning is adjusted [18]), exists in such system. However, the contributions of the mutual dressing effects can be an order of magnitude larger than the interference effect in such a system [17].

In the open five-level system studied here, several features are different and advantageous over the previously reported multiwave mixing processes [1–9]. First, there coexist DDFWM (with three dressing schemes), singly dressed SWM (DSWM), and EWM in this open five-level system. This is a good system for studying the interplays between nonlinear optical processes of different orders. Second, three DDFWM processes (in nested-cascade, parallel-cascade, and sequential-cascade schemes) and their relationships can be considered in detail. By careful comparisons, we find that the interaction between two dressing processes in the nested-cascade scheme is the strongest and that in the parallel-cascade scheme is the weakest. The sequential-cascade scheme is an intermediate between those above two schemes. Third, we have investigated the Aulter-Townes (AT) splitting and suppression or enhancement of FWM spectra that can be interpreted by both dressed-state diagrams and competitions between dispersion and absorption of the dressed MWM. Fourth, by virtue of controlling the DSWM or DDFWM signal, mutual dressing processes and constructive or destructive interference existing in this open five-level system are considered. Investigations of such intermixing and interplays

*ypzhang@mail.xjtu.edu.cn

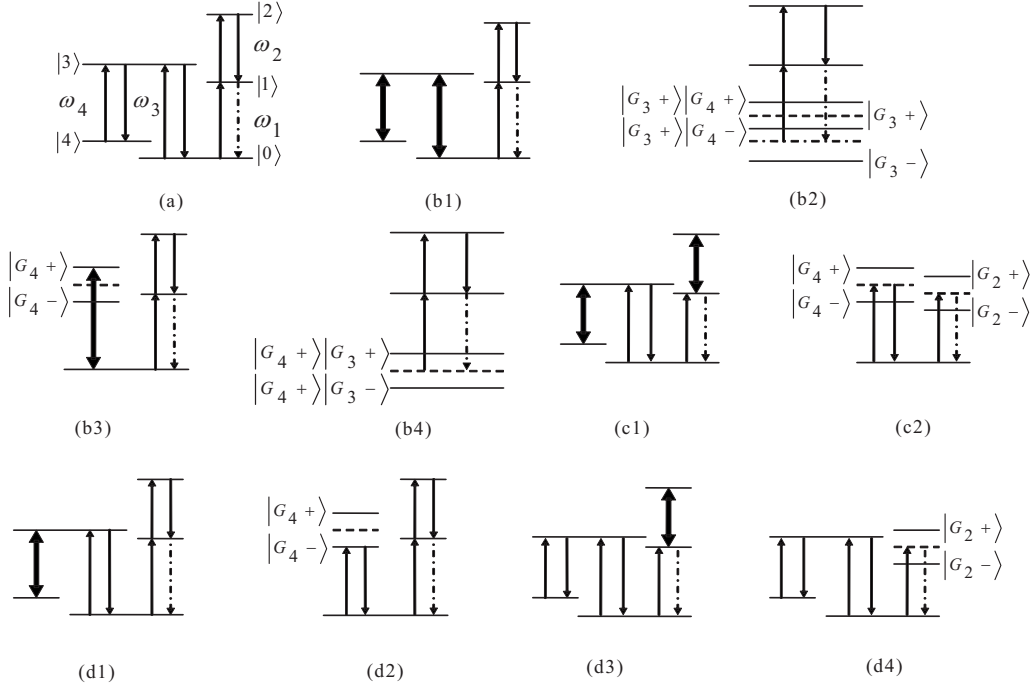


FIG. 1. (a) Energy-level diagram of an open five-level system for EWM. (b1) Nested-cascade DDFWM and (b2)–(b4) the dressed-state pictures. (c1) Parallel- and sequential-cascade DDFWM and (c2) the dressed-state picture for parallel-cascade DDFWM. (d1) and (d3) Two DSWM and the (d2) and (d4) dressed-state pictures.

between different types of nonlinear wave-mixing processes will help us to understand and optimize the generated high-order multichannel nonlinear optical signals, which have potential applications in achieving better nonlinear optical materials and optoelectronic devices (for example, all optical-switch or controlled-NOT gate).

The paper is organized as follows. Section II presents general calculations to describe the three doubly dressing (i.e., nested-cascade, sequential-cascade, and parallel-cascade) schemes of DDFWM. Section III shows AT splitting, suppression, or enhancement of FWM signal intensity for each doubly dressing scheme. Section IV studies the competitions between two coexisting dressed MWM processes. Finally, Sec. V gives the conclusion.

II. THREE DOUBLY DRESSING SCHEMES

Let us consider an open five-level system as shown in Fig. 1(a). In the $|0\rangle$ – $|1\rangle$ – $|2\rangle$ subsystem, the beam E_1 (ω_1 , k_1 , and Rabi frequency G_1) probes the lower transition $|0\rangle$ to $|1\rangle$ while two coupling beams, E_2 (ω_2 , k_2 , and G_2) and E_2' (ω_2 , k_2' , and G_2'), drive the transition $|1\rangle$ to $|2\rangle$. One FWM signal field E_{f1} (ω_1 , $\mathbf{k}_{f1}=\mathbf{k}_1+\mathbf{k}_2-\mathbf{k}_2'$) will be generated via the FWM perturbation chain (f1) $\rho_{00}^{(0)} \rightarrow \rho_{10}^{(1)} \rightarrow \rho_{20}^{(2)} \rightarrow \rho_{10}^{(3)}$ and gives

$$\rho_{f1} = \rho_{10}^{(3)} = -iG_A \exp(i\mathbf{k}_{f1} \cdot \mathbf{r})/d_1^2 d_2, \quad (1)$$

where $G_A = G_1 G_2 (G_2')^*$, $d_1 = \Gamma_{10} + i\Delta_1$, and $d_2 = \Gamma_{20} + i(\Delta_1 + \Delta_2)$ with frequency detuning $\Delta_i = \Omega_i - \omega_i$. Γ_{ij} is the transverse relaxation rate between states $|i\rangle$ and $|j\rangle$. Ω_i is the atomic resonance frequency.

Similarly, in the $|3\rangle$ – $|0\rangle$ – $|1\rangle$ subsystem, the FWM process, using one photon each from E_1 , E_3 (ω_3 , \mathbf{k}_3 , G_3), and E_3' (ω_3 , \mathbf{k}_3' , G_3') (driving the transition $|0\rangle$ to $|3\rangle$), generates another signal field E_{f2} (ω_1 , $\mathbf{k}_{f2}=\mathbf{k}_1+\mathbf{k}_3-\mathbf{k}_3'$) via another FWM chain (f2) $\rho_{00}^{(0)} \rightarrow \rho_{10}^{(1)} \rightarrow \rho_{13}^{(2)} \rightarrow \rho_{10}^{(3)}$ and gives

$$\rho_{f2} = \rho_{10}^{(3)} = -iG_B \exp(i\mathbf{k}_{f2} \cdot \mathbf{r})/d_1^2 d_3, \quad (2)$$

where $G_B = G_1 G_3 G_3'^*$, $d_3 = \Gamma_{13} + i(\Delta_1 - \Delta_3)$.

On the other hand, there also coexist SWM processes in different four-level subsystems and EWM processes in the five-level system via the SWM and EWM perturbation chains [15,16]. All these chains are quite helpful for investigating the interactions in the DDFWM processes.

In such a five-level open atomic system, we apply two additional strong-coupling fields to dress the FWM processes. As a result, DDFWM processes with three different doubly dressing (nested cascade, parallel cascade, and sequential cascade) schemes are obtained [19,20].

A. Nested-cascade DDFWM

For nested-cascade DDFWM, the outer dressing field E_4 (ω_4 , \mathbf{k}_4 , G_4) drives the transition from $|3\rangle$ to $|4\rangle$, and the inner dressing field E_3 dresses the level $|0\rangle$ [Fig. 1(b1)] via a segment (subchain) of the EWM perturbation chain (e1) $\rho_{00}^{(0)} \rightarrow \rho_{10}^{(1)} \rightarrow \rho_{20}^{(2)} \rightarrow \rho_{23}^{(3)} \rightarrow \rho_{24}^{(4)} \rightarrow \rho_{23}^{(5)} \rightarrow \rho_{20}^{(6)} \rightarrow \rho_{10}^{(7)}$. In detail, the subchain $\rho_{23}^{(3)} \rightarrow \rho_{24}^{(4)} \rightarrow \rho_{23}^{(5)}$ (related to the dressing field E_4) is nested between the subchains $\rho_{20}^{(2)} \rightarrow \rho_{23}^{(3)}$ and $\rho_{23}^{(5)} \rightarrow \rho_{20}^{(6)}$ due to the dressing field E_3 . Hence, such a doubly dressing scheme

is denoted as the nested-cascade scheme. By virtue of the perturbation chain (e1), we can modify the FWM chain (f1) to give the DDFWM chain (Df1) $\rho_{00}^{(0)} \xrightarrow{\omega_1} \rho_{10}^{(1)} \xrightarrow{\omega_2} \rho_{2(G_4 \pm G_3 \pm)}^{(2)} \xrightarrow{-\omega_2} \rho_{10}^{(3)}$. Here the subscript “0” of $\rho_{20}^{(2)}$ in (f1) is replaced by “ $G_4 \pm G_3 \pm$ ” in (Df1), which indicates that two dressing fields dress the level $|0\rangle$ and influence the identical coherence between states $|0\rangle$ and $|2\rangle$.

According to the chain (Df1), we can obtain the equations for the dressed FWM processes $\rho_{10}^{(1)} = iG_1 \exp(i\mathbf{k}_1 \cdot \mathbf{r}) \rho_{00}^{(0)} / d_1$ and $\rho_{10}^{(3)} = iG_2^* \exp(-i\mathbf{k}_2' \cdot \mathbf{r}) \rho_{2(G_4 \pm G_3 \pm)}^{(2)} / d_1$. On the other hand, the perturbation approach for such dressing cases can be well described by the following coupled equations:

$$\begin{aligned} \partial \rho_{20}^{(2)} / \partial t &= -d_2 \rho_{20}^{(2)} + iG_2 \exp(i\mathbf{k}_2 \cdot \mathbf{r}) \rho_{10}^{(1)} \\ &\quad - iG_3 \exp(i\mathbf{k}_3 \cdot \mathbf{r}) \rho_{23}, \\ \partial \rho_{23} / \partial t &= -d_4 \rho_{23} - iG_3^* \exp(-i\mathbf{k}_3 \cdot \mathbf{r}) \rho_{20}^{(2)} \\ &\quad - iG_4^* \exp(-i\mathbf{k}_4 \cdot \mathbf{r}) \rho_{24}, \\ \partial \rho_{24} / \partial t &= -d_5 \rho_{24} - iG_4 \exp(i\mathbf{k}_4 \cdot \mathbf{r}) \rho_{23}. \end{aligned}$$

Here, $d_4 = \Gamma_{23} + i(\Delta_1 + \Delta_2 - \Delta_3)$ and $d_5 = \Gamma_{24} + i(\Delta_1 + \Delta_2 - \Delta_3 + \Delta_4)$. In the steady state, $\partial \rho_{20}^{(2)} / \partial t = \partial \rho_{23} / \partial t = \partial \rho_{24} / \partial t = 0$, we have

$$\rho_{2(G_4 \pm G_3 \pm)}^{(2)} = \rho_{20}^{(2)} = \frac{iG_2 \exp(i\mathbf{k}_2 \cdot \mathbf{r}) \rho_{10}^{(1)}}{d_2 + \frac{G_3^2}{d_4 + G_4^2/d_5}}.$$

On the condition of $\rho_{00}^{(0)} = 1$ (which is a reasonable assumption since the probe field is always assumed to be weak comparing to other fields), we finally obtain

$$\rho_{\text{Df1}} = \rho_{10}^{(3)} = \frac{-iG_A \exp(i\mathbf{k}_{f1} \cdot \mathbf{r})}{d_1^2 \left(d_2 + \frac{|G_3|^2}{d_4 + |G_4|^2/d_5} \right)}. \quad (3)$$

In fact, without these dressing fields ($G_3 = G_4 = 0$), Eq. (3) can be converted into Eq. (1). The item “ d_2 ” representing the “ $\omega_1 + \omega_2$ ” two-photon process of ρ_{f1} is modified directly by the intensity $|G_3|^2$, while $|G_3|^2$ is modified by the intensity $|G_4|^2$. Hence Eq. (3) shows that the two dressing fields are entangled with each other for such a nested-cascade scheme. The inner dressing field E_3 controls FWM directly, while the outer dressing field E_4 controls FWM only indirectly. Moreover, in the weak-dressing-field limit ($|G_3|^2 \ll \Gamma_{20}\Gamma_{23}$ and $|G_4|^2 \ll \Gamma_{23}\Gamma_{24}$), Eq. (3) can be expanded to be [21]

$$\rho_{\text{Df1}} = \rho_{f1} + \rho_{s1} + \rho_{e1}. \quad (4)$$

Here, $\rho_{s1} = iG_A |G_3|^2 \exp(i\mathbf{k}_{s1} \cdot \mathbf{r}) / (d_1^2 d_2^2 d_4)$ with $\mathbf{k}_{s1} = \mathbf{k}_{f1} + \mathbf{k}_3 - \mathbf{k}_3$ and $\rho_{e1} = -iG_A |G_3|^2 |G_4|^2 \exp(i\mathbf{k}_{e1} \cdot \mathbf{r}) / (d_1^2 d_2^2 d_4^2 d_5)$ with $\mathbf{k}_{e1} = \mathbf{k}_{f1} + \mathbf{k}_3 - \mathbf{k}_3 + \mathbf{k}_4 - \mathbf{k}_4$ are the expressions for the SWM and EWM processes, respectively. Equation (4) shows that the nested-cascade DDFWM is a coherent superposition of the signals from FWM, SWM, and EWM under the weak-dressing-field condition.

B. Parallel-cascade DDFWM

For parallel-cascade DDFWM, as shown in Fig. 1(c1), the dressing fields E_2 and E_4 dress the levels $|1\rangle$ and $|3\rangle$, respectively, via the subchains of the EWM chain (e2) $\rho_{00}^{(0)} \xrightarrow{\omega_1} \rho_{10}^{(1)} \xrightarrow{\omega_2} \rho_{20}^{(2)} \xrightarrow{-\omega_2} \rho_{10}^{(3)} \xrightarrow{-\omega_3} \rho_{13}^{(4)} \xrightarrow{\omega_4} \rho_{14}^{(5)} \xrightarrow{-\omega_4} \rho_{13}^{(6)} \xrightarrow{\omega_3} \rho_{10}^{(7)}$. Two subchains of the dressing fields “ $\rho_{10}^{(1)} \xrightarrow{\omega_2} \rho_{20}^{(2)} \xrightarrow{-\omega_2} \rho_{10}^{(3)}$ ” (for E_2) and “ $\rho_{13}^{(4)} \xrightarrow{\omega_4} \rho_{14}^{(5)} \xrightarrow{-\omega_4} \rho_{13}^{(6)}$ ” (for E_4) lie parallel within the chain (e2) and such a doubly dressing scheme is denoted as a parallel-cascade scheme. The FWM chain (f2) is modified by the DDFWM chain (Df2) as $\rho_{00}^{(0)} \xrightarrow{\omega_1} \rho_{G2\pm 0}^{(1)} \xrightarrow{-\omega_3} \rho_{1G4\pm}^{(2)} \xrightarrow{\omega_3} \rho_{10}^{(3)}$. Here the subscripts “1” of $\rho_{10}^{(1)}$ and “3” of $\rho_{13}^{(2)}$ in (f2) are replaced by “ $G_2 \pm$ ” and “ $G_4 \pm$ ” in (Df2), respectively. These two dressing fields now dress different energy levels and influence different coherences $\rho_{10}^{(1)}$ and $\rho_{13}^{(2)}$ of the FWM processes.

According to the perturbation chain (Df2), we obtain the equation for the modified FWM $\rho_{10}^{(3)} = -iG_3 \times \exp(i\mathbf{k}_3 \cdot \mathbf{r}) \rho_{1G4\pm}^{(2)} / d_1$ and the coupled equations

$$\begin{aligned} \partial \rho_{10}^{(1)} / \partial t &= -d_1 \rho_{10}^{(1)} + iG_1 \exp(i\mathbf{k}_1 \cdot \mathbf{r}) \rho_{00}^{(0)} \\ &\quad + iG_2^* \exp(-i\mathbf{k}_2 \cdot \mathbf{r}) \rho_{20}, \end{aligned}$$

$$\partial \rho_{20} / \partial t = -d_2 \rho_{20} + iG_2 \exp(i\mathbf{k}_2 \cdot \mathbf{r}) \rho_{10}^{(1)},$$

$$\begin{aligned} \partial \rho_{13}^{(2)} / \partial t &= -d_3 \rho_{13}^{(2)} - iG_3^* \exp(-i\mathbf{k}_3' \cdot \mathbf{r}) \rho_{10}^{(1)} \\ &\quad - iG_4^* \exp(-i\mathbf{k}_4 \cdot \mathbf{r}) \rho_{14}, \end{aligned}$$

$$\partial \rho_{14} / \partial t = -d_6 \rho_{14} - iG_4 \exp(i\mathbf{k}_4 \cdot \mathbf{r}) \rho_{13}^{(2)}.$$

Here $d_6 = \Gamma_{14} + i(\Delta_1 - \Delta_3 + \Delta_4)$. In the steady state $\partial \rho_{10}^{(1)} / \partial t = \partial \rho_{20} / \partial t = \partial \rho_{13}^{(2)} / \partial t = \partial \rho_{14} / \partial t = 0$, we have

$$\rho_{G2\pm 0}^{(1)} = \rho_{10}^{(1)} = \frac{iG_1 \exp(i\mathbf{k}_1 \cdot \mathbf{r})}{d_1 + |G_2|^2/d_2} \rho_{00}^{(0)}$$

and

$$\rho_{1G4\pm}^{(2)} = \rho_{13}^{(2)} = \frac{-iG_3^* \exp(-i\mathbf{k}_3' \cdot \mathbf{r})}{d_3 + |G_4|^2/d_6} \rho_{10}^{(1)}.$$

With $\rho_{00}^{(0)} = 1$, we can solve the above equations to obtain

$$\rho_{\text{Df2}} = \rho_{10}^{(3)} = \frac{-iG_B \exp(i\mathbf{k}_{f2} \cdot \mathbf{r})}{d_1(d_3 + |G_4|^2/d_6)(d_1 + |G_2|^2/d_2)}. \quad (5)$$

Comparing with Eq. (2), the items d_3 and d_1 in Eq. (5) are modified by the intensities of the dressing fields $|G_2|^2$ and $|G_4|^2$, respectively. In the weak-dressing-field limit ($|G_2|^2 \ll \Gamma_{10}\Gamma_{20}$ and $|G_4|^2 \ll \Gamma_{13}\Gamma_{14}$), Eq. (3) can be expanded to be

$$\rho_{\text{Df2}} = \rho_{f2} + \rho_{s2} + \rho_{s3} + \rho_{e2}. \quad (6)$$

Here $\rho_{s2} = i|G_2|^2 G_B \exp(i\mathbf{k}_{s2} \cdot \mathbf{r}) / (d_1^2 d_2^2 d_3)$ with $\mathbf{k}_{s2} = \mathbf{k}_{f2} + \mathbf{k}_2 - \mathbf{k}_2$, $\rho_{s3} = i|G_4|^2 G_B \exp(i\mathbf{k}_{s3} \cdot \mathbf{r}) / (d_1^2 d_3^2 d_6)$ with $\mathbf{k}_{s3} = \mathbf{k}_{f2} + \mathbf{k}_4 - \mathbf{k}_4$, and $\rho_{e2} = -i|G_2|^2 |G_4|^2 G_B \exp(i\mathbf{k}_{e2} \cdot \mathbf{r}) / (d_1^3 d_2^2 d_3^2 d_6)$ with $\mathbf{k}_{e2} = \mathbf{k}_{f2} + \mathbf{k}_2 - \mathbf{k}_2 + \mathbf{k}_4 - \mathbf{k}_4$ are the expressions for SWM and EWM processes, respectively. This means that under the weak-dressing-field condition, the parallel-cascade DDFWM

can be considered as a coherent superposition of the signals from one FWM process, two SWM processes, and one EWM process.

C. Sequential-cascade DDFWM

For the sequential-cascade DDFWM, the energy-level diagram is the same as the parallel-cascade DDFWM [Fig. 1(c1)]. However, the two dressing fields E_2 and E_4 dress ρ_{f2} via the subchains of a different EWM perturbation chain (e3) $\rho_{00}^{(0)} \xrightarrow{\omega_1} \rho_{10}^{(1)} \xrightarrow{-\omega_3} \rho_{13}^{(2)} \xrightarrow{\omega_2} \rho_{23}^{(3)} \xrightarrow{-\omega_2} \rho_{13}^{(4)} \xrightarrow{\omega_4} \rho_{14}^{(5)} \xrightarrow{-\omega_4} \rho_{13}^{(6)} \xrightarrow{\omega_3} \rho_{10}^{(7)}$. Note that the two subchains of the dressing fields $\rho_{13}^{(2)} \xrightarrow{\omega_2} \rho_{23}^{(3)} \xrightarrow{-\omega_2} \rho_{13}^{(4)}$ and $\rho_{13}^{(4)} \xrightarrow{\omega_4} \rho_{14}^{(5)} \xrightarrow{-\omega_4} \rho_{13}^{(6)}$ join together sequentially. Such a doubly dressing scheme is denoted as the sequential-cascade scheme. According to the chain (e3), the FWM chain (f2) is modified by the DDFWM to be (Df3) $\rho_{00}^{(0)} \xrightarrow{\omega_1} \rho_{10}^{(1)} \xrightarrow{-\omega_3} \rho_{G_2 \pm G_4 \pm}^{(2)} \xrightarrow{\omega_3} \rho_{10}^{(3)}$. Here the subscripts “1” and “3” of $\rho_{13}^{(2)}$ in (f2) are replaced by “ $G_2 \pm$ ” and “ $G_4 \pm$ ” in (Df3), respectively. This means that the two dressing fields dress different energy levels, but they influence the same coherence between states |1⟩ and |3⟩. Similarly, from the chain (Df3) we have the equations $\rho_{10}^{(1)} = iG_1 \exp(i\mathbf{k}_1 \cdot \mathbf{r}) \rho_{00}^{(0)} / d_1$ and $\rho_{10}^{(3)} = -iG_3 \times \exp(i\mathbf{k}_3 \cdot \mathbf{r}) \rho_{G_2 \pm G_4 \pm}^{(2)} / d_1$, and the coupled equations

$$\begin{aligned} \partial \rho_{13}^{(2)} / \partial t &= -d_3 \rho_{13}^{(2)} + iG_2^* \exp(-i\mathbf{k}_2 \cdot \mathbf{r}) \rho_{23} \\ &\quad - iG_3^* \exp(-i\mathbf{k}_3 \cdot \mathbf{r}) \rho_{10}^{(1)} - iG_4^* \exp(-i\mathbf{k}_4 \cdot \mathbf{r}) \rho_{14}, \\ \partial \rho_{23} / \partial t &= -d_4 \rho_{23} + iG_2 \exp(i\mathbf{k}_2 \cdot \mathbf{r}) \rho_{13}^{(2)}, \\ \partial \rho_{14} / \partial t &= -d_6 \rho_{14} - iG_4 \exp(i\mathbf{k}_4 \cdot \mathbf{r}) \rho_{13}^{(2)}. \end{aligned}$$

In the steady state, $\partial \rho_{13}^{(2)} / \partial t = \partial \rho_{23} / \partial t = \partial \rho_{14} / \partial t = 0$ and we obtain

$$\rho_{G_2 \pm G_4 \pm}^{(2)} = \rho_{13}^{(2)} = \frac{-iG_3^* \exp(-i\mathbf{k}_3 \cdot \mathbf{r})}{d_3 + |G_2|^2/d_4 + |G_4|^2/d_6} \rho_{10}^{(1)},$$

which, under $\rho_{00}^{(0)} = 1$, gives

$$\rho_{\text{Df3}} = \rho_{10}^{(3)} = \frac{-iG_B \exp(i\mathbf{k}_{f2} \cdot \mathbf{r})}{d_1^2(d_3 + |G_2|^2/d_4 + |G_4|^2/d_6)}. \quad (7)$$

Comparing with Eq. (2), the item “ d_3 ” in Eq. (7) is modified by the intensities G_2 and G_4 together. Again, in the weak-dressing-field limit ($|G_2|^2 \ll \Gamma_{13}\Gamma_{23}$ and $|G_4|^2 \ll \Gamma_{13}\Gamma_{14}$), Eq. (7) can be expanded to be

$$\rho_{\text{Df3}} = \rho_{f2} + \rho_{s3} + \rho_{s4}, \quad (8)$$

which indicates that the sequential-cascade DDFWM can be considered as a coherent superposition of the signals from one FWM and two SWM processes. Here $\rho_{s4} = i|G_2|^2 G_B \exp(i\mathbf{k}_{s2} \cdot \mathbf{r}) / (d_1^2 d_3^2 d_4)$ is an expression for SWM.

DDFWM processes with two dressing fields have been investigated above for three different doubly dressing schemes, which present different interactions between the two dressing fields and the FWM channels. In the following, we discuss and present the major differences and similarities of these different doubly dressing schemes.

First, in terms of the energy level diagrams, the two dressing fields in the nested-cascade scheme connect three neighboring levels in the subsystem $|0\rangle - |3\rangle - |4\rangle$ and the outer dressing field is based on the inner dressing field while the inner one dresses the state $|0\rangle$ [Fig. 1(b1)]. However, the dressing fields in the parallel-cascade and sequential-cascade schemes dress two different states directly and independently [Fig. 1(c1)].

Second, the dissimilarities among the DDFWM perturbation chains also represent the differences between the three doubly dressing schemes. In the nested-cascade scheme, the two dressing fields are entangled tightly with each other according to the subchain $\rho_{20}^{(2)} \xrightarrow{-\omega_3} \rho_{23}^{(3)} \xrightarrow{\omega_4} \rho_{24}^{(4)} \xrightarrow{-\omega_4} \rho_{23}^{(5)} \xrightarrow{\omega_3} \rho_{20}^{(6)}$ in the chain (e1). However, for the parallel-cascade scheme, the two dressing processes “ $\rho_{10}^{(1)} \xrightarrow{\omega_2} \rho_{20}^{(2)} \xrightarrow{-\omega_2} \rho_{10}^{(3)}$ ” and “ $\rho_{13}^{(4)} \xrightarrow{\omega_4} \rho_{14}^{(5)} \xrightarrow{-\omega_4} \rho_{13}^{(6)}$ ” are separated in the chain (e2) (not connected). For the sequential-cascade scheme, although “ $\rho_{13}^{(2)} \xrightarrow{\omega_2} \rho_{23}^{(3)} \xrightarrow{-\omega_2} \rho_{13}^{(4)}$ ” and “ $\rho_{13}^{(4)} \xrightarrow{\omega_4} \rho_{14}^{(5)} \xrightarrow{-\omega_4} \rho_{13}^{(6)}$ ” lie independently in the perturbation chain (e3), they are conjoined by $\rho_{13}^{(4)}$ in the chain. This means that the interaction between the two dressing fields in the nested-cascade scheme is the strongest and the interaction in the parallel-cascade scheme is the weakest. The sequential-cascade scheme is an intermediate case between them.

Third, according to the DDFWM expressions, for the nested-cascade DDFWM in Eq. (3) if $|G_3|^2 = 0$, $|G_4|^2$ (the dressing field E_4) will have no effect on the result. However, the intensities of the dressing fields are independent for both parallel- and sequential-cascade DDFWM cases, as can be seen in Eqs. (5) and (7). On the other hand, only one term of FWM is modified by the dressing fields for the nested- and sequential-cascade schemes, while two terms are modified for the parallel-cascade scheme. In fact, the forms of the nested- and parallel-cascade DDFWM expressions can be converted into the form of the sequential-cascade DDFWM one under certain conditions, which shows that the sequential-cascade scheme is an intermediate case between the above two schemes. In the limit of small G_4 or large Δ_4 , Eq. (3) can be written as

$$\rho_{\text{Df1}} \approx \frac{-iG_A \exp(i\mathbf{k}_{f1} \cdot \mathbf{r})}{d_1^2 [d_2 + |G_3|^2/d_4 + |G_4|^2/D(\Delta_4)]}, \quad (9)$$

where $D(\Delta_4) = -d_4^2 d_5 / |G_3|^2$. Thus, the form of Eq. (9) is the same as that of Eq. (7). Also, according to Eq. (6) of the parallel-cascade DDFWM, if $|G_2|^2$ and $|G_4|^2$ are small enough, the EWM term ρ_{e2} can be ignored and we are left with

$$\rho_{\text{Df2}} \approx \rho_{f2} + \rho_{s2} + \rho_{s3}, \quad (10)$$

which is similar to Eq. (8) for the sequential-cascade DDFWM. Hence, the weaker the dressing fields are, the more alike the parallel- and sequential-cascade DDFWM processes will become.

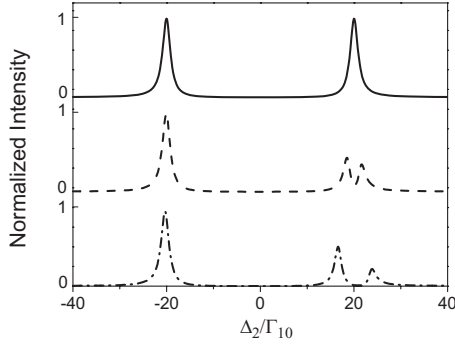


FIG. 2. Nested-cascade DDFWM signal intensity versus Δ_2/Γ_{10} for $\Delta_1=\Delta_3=0$, $G_3/\Gamma_{10}=20$, $G_4/\Gamma_{10}=2$, $\Delta_4/\Gamma_{10}=2000$ (solid curve); $\Delta_4/\Gamma_{10}=-20$ (dashed curve); and $G_4/\Gamma_{10}=5$, $\Delta_4/\Gamma_{10}=-20$ (dot-dashed curve). The other parameters are $\Gamma_{20}/\Gamma_{10}=0.8$, $\Gamma_{23}/\Gamma_{10}=1.2$, and $\Gamma_{24}/\Gamma_{10}=0.8$. The maximum of the intensity is normalized to be 1.

From these discussions we can conclude that the interaction between two dressing processes is strongest in the nested-cascade scheme and weakest in the parallel-cascade scheme.

III. AULTER-TOWNES SPLITTING, SUPPRESSION, AND ENHANCEMENT

One possible experimental candidate for the proposed system is ^{85}Rb atoms with states $|0\rangle=|5S_{1/2}\rangle$ ($F=2$), $|1\rangle=|5P_{1/2}\rangle$, $|2\rangle=|5D_{3/2}\rangle$, $|3\rangle=|5P_{3/2}\rangle$, and $|4\rangle=|5S_{1/2}\rangle$ ($F=3$). The respective transitions are $|0\rangle\rightarrow|1\rangle$ at 795 nm [$\gamma_{10}\approx 5.4$ MHz, where γ_{ij} gives decay due to spontaneous emission (longitudinal relaxation rate) between states $|i\rangle$ and $|j\rangle$], $|1\rangle\rightarrow|2\rangle$ at 762 nm ($\gamma_{21}\approx 0.98$ MHz), $|0\rangle\rightarrow|3\rangle$ at 780 nm ($\gamma_{30}\approx 5.9$ MHz), $|3\rangle\rightarrow|4\rangle$ at 780 nm ($\gamma_{34}\approx 5.9$ MHz), $|4\rangle\rightarrow|1\rangle$ at 795 nm ($\gamma_{14}\approx 5.4$ MHz), and $|3\rangle\rightarrow|2\rangle$ at 776 nm ($\gamma_{23}\approx 0.8$ MHz). The transverse relaxation rate Γ_{ij} between states $|i\rangle$ and $|j\rangle$ is given by $\Gamma_{ij}=(\Gamma_i+\Gamma_j)/2$ ($\Gamma_0=\gamma_{40}$, $\Gamma_1=\gamma_{10}+\gamma_{14}$, $\Gamma_2=\gamma_{21}+\gamma_{23}$, $\Gamma_3=\gamma_{30}+\gamma_{34}$, and $\Gamma_4=\gamma_{40}$). Here the nonlinear polarizations in such a five-level system inter-

act with up to seven laser fields. We assume that the Rabi frequency G_1 is small while G_2 , G'_2 , G_3 , G'_3 , G_4 , and G'_4 can be of arbitrary magnitudes [7–9,16,17]. In this section, we will plot the normalized DDFWM signal intensities based on the analytic expressions shown above.

A. Nested-cascade DDFWM

We first investigate the spectra of the nested-cascade DDFWM. Figure 2 presents the signal intensity versus the pump field detuning Δ_2 corresponding to the primarily dressed states and the secondarily dressed states, as shown in Fig. 1(b2). According to Eq. (3), in the solid curve, the inner dressing field E_3 splits the “ $\omega_1+\omega_2$ ” two-photon resonant peak into two peaks located at $\Delta_2=\pm\Delta_{G_3}/2\approx\pm G_3$ under the condition $|G_3|^2\gg\Gamma_{20}\Gamma_{23}$, which is the primary AT splitting. Here Δ_{G_3} is the separation induced by the dressing field E_3 . The outer dressing field E_4 with a large detuning has almost no impact in this case. According to dressed-state analysis, the right and left peaks represent the transitions from the two primarily dressed states $|G_3+\rangle$ and $|G_3-\rangle$, separated from the ground state $|0\rangle$ to the exciting state $|2\rangle$. More importantly, when the outer dressing field E_4 dresses the primarily dressed state $|G_3+\rangle$ ($\Delta_4=-G_3$) and becomes stronger, the dashed and dotted curves show the secondary AT splitting of the right peak, which represents that $|G_3+\rangle$ is separated into the secondary dressed states $|G_3+\rangle|G_4\pm\rangle$ [Fig. 1(b2)].

Next, we investigate the spectra versus the inner dressing field detuning Δ_3 while keeping the pump field detuning fixed. Figure 3 shows the impact of the two dressing fields on the FWM signal intensity. Here the FWM signal intensity with no dressing fields ($G_3=G_4=0$) is normalized to 1. The intensity above or below “1” means enhancement or suppression of the FWM signal. Figure 3(a) shows that there is a suppressed dip at the line center first. As G_4 is increased, this dip becomes shallow and then splits into two dips. In the limit of $G_4\gg\Gamma_{23},\Gamma_{24}$ we have $\Delta_{G_4}\approx 2G_4$. Here, Δ_{G_4} is the separation induced by the dressing field E_4 . This means that the inner dressing field E_3 suppresses the resonant FWM

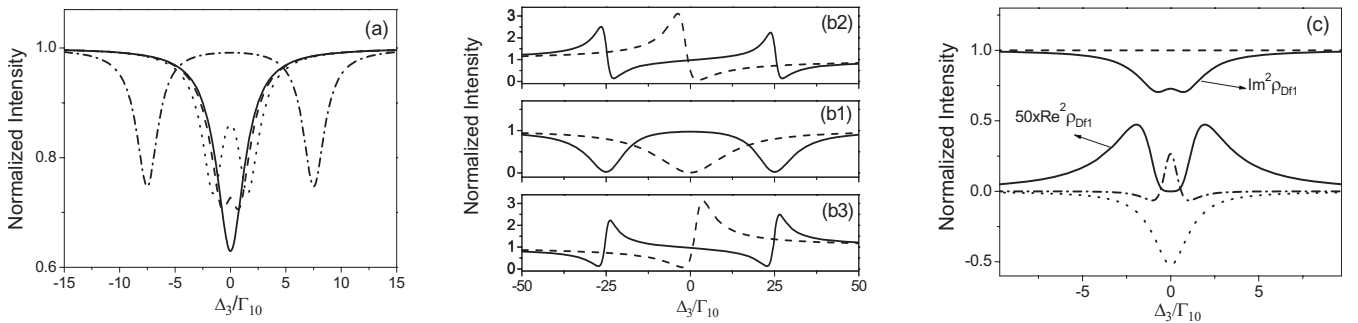


FIG. 3. Nested-cascade DDFWM signal intensity versus Δ_3/Γ_{10} for (a) $\Delta_1=\Delta_2=\Delta_4=0$, $G_3/\Gamma_{10}=0.5$, $G_4/\Gamma_{10}=0$ (solid curve), $G_4/\Gamma_{10}=0.7$ (dashed curve), $G_4/\Gamma_{10}=1.5$ (dotted curve), $G_4/\Gamma_{10}=7.5$ (dot-dashed curve); (b1) $\Delta_2=\Delta_4=0$, $G_3/\Gamma_{10}=3$, $\Delta_1/\Gamma_{10}=2$, $G_4/\Gamma_{10}=25$ (solid curve), $G_4/\Gamma_{10}=0$ (dashed curve); (b2) $\Delta_2=\Delta_4=0$, $G_3/\Gamma_{10}=3$, $\Delta_1/\Gamma_{10}=2$, $G_4/\Gamma_{10}=25$ (solid curve), $G_4/\Gamma_{10}=0$ (dashed curve); (b3) $\Delta_2=\Delta_4=0$, $G_3/\Gamma_{10}=3$, $\Delta_1=-2$, $G_4/\Gamma_{10}=25$ (solid curve), $G_4/\Gamma_{10}=0$ (dashed curve); (c) the values of $\text{Re}^2\rho_{DF1}$ scaled by a factor 50, $\text{Im}^2\rho_{DF1}$, $\text{Im}\rho_{F1}\text{Im}\rho_{s3}$ (dotted curve), and $\text{Im}\rho_{F1}\text{Im}\rho_{e5}$ (dot-dashed curve) versus Δ_3/Γ_{10} for $G_3/\Gamma_{10}=0.5$, $G_4/\Gamma_{10}=0.7$, $\Delta_1=\Delta_2=\Delta_4=0$. The other common parameters are $\Gamma_{20}/\Gamma_{10}=0.8$, $\Gamma_{23}/\Gamma_{10}=1.2$, $\Gamma_{24}/\Gamma_{10}=0.8$. The FWM signal intensity with no dressing fields is normalized to be 1.

signal directly and creates one suppressed dip while the outer dressing field E_4 splits that suppressed dip to create a pair of FWM channels.

As G_4 becomes large, the two channels are significantly apart as shown in the solid curves of Fig. 3(b). Through such a pair of channels, the inner dressing field E_3 can doubly suppress the resonant FWM signal [the solid curve in Fig. 3(b1)] and doubly suppress or enhance the off-resonant FWM signals [the solid curves in Figs. 3(b2) and (b3)], respectively. However, without the outer dressing field E_4 there only exists one suppressed dip [the dashed curves in Figs. 3(b1)—(b3)] and one enhanced peak [the dashed curves in Figs. 3(b2) and (b3)]. The outer dressing field E_4 splits the peaks and dips in the dashed curves into the dual-enhanced peaks and dual-suppressed dips in the solid curves, respectively.

The dressed-state analysis agrees well with Fig. 3(b). If $G_4=0$, only the dressing field E_3 drives the transition from $|3\rangle$ to $|0\rangle$ and creates the dressed states $|G_3\pm\rangle$ from $|0\rangle$. Thus the “ $\omega_1+\omega_2$ ” two-photon resonant or off-resonant transition of FWM ρ_{f1} gets off-resonant or more off-resonant, which results in a suppression of the FWM signal intensity as shown by the dips in the dashed curve of Fig. 3(b). Hence we can deduce the suppressed-dip condition $\omega_1+\omega_2-\omega_3=\Omega_1+\Omega_2-\Omega_3$ (i.e., $\Delta_3=\Delta_1+\Delta_2=0$ or ± 2). On the other hand, the dressed state $|G_3+\rangle$ can make the off-resonant transition resonant, and the FWM signal intensity is enhanced as shown by the peak of the dashed curve in Fig. 3(b2) at $\omega_1+\omega_2-\omega_3\approx(\Omega_1-\Delta_{G3}/2)+\Omega_2-\Omega_3$ (i.e., $\Delta_3\approx\Delta_1+\Delta_2-\Delta_{G3}/2\approx-3.8$). Similarly, the enhanced peak of the dashed curve in Fig. 3(b3) is induced by the other dressed state $|G_3-\rangle$ if $\omega_1+\omega_2-\omega_3\approx(\Omega_1+\Delta_{G3}/2)+\Omega_2-\Omega_3$ (i.e., $\Delta_3\approx\Delta_1+\Delta_2+\Delta_{G3}/2\approx 3.8$). Here, we assume that $|G_3\pm\rangle$ are created symmetrically.

As G_4 is quite large, the outer dressing field E_4 dresses the level $|3\rangle$ and creates the primarily dressed states $|G_4\pm\rangle$, as shown in Fig. 1(b3). The inner dressing field E_3 , driving the transitions from $|G_4\pm\rangle$ to the ground level $|0\rangle$, creates the secondarily dressed states $|G_4+\rangle|G_3\pm\rangle$ [Fig. 1(b4)] or $|G_4-\rangle|G_3\pm\rangle$ from $|0\rangle$ to cause the two-photon resonant and off-resonant transitions of ρ_{f1} to be off-resonant or more off-resonant [Fig. 1(b4)], which induces two suppressed dips in the solid curve of Fig. 3(b) under the condition of $\omega_1+\omega_2-\omega_3+\omega_4\approx\Omega_1+\Omega_2-(\Omega_3\pm\Delta_{G4}/2)+\Omega_4$ [i.e., $\Delta_3\approx\Delta_1+\Delta_2+\Delta_4\pm\Delta_{G4}/2=0\pm 25$ for Fig. 3(b1), or 2 ± 25 for Fig. 3(b2), or -2 ± 25 for Fig. 3(b3)]. Here, we assume the primarily dressed states $|G_4\pm\rangle$ are created symmetrically. On the other hand, the secondarily dressed states $|G_4\pm\rangle|G_3+\rangle$ can cause resonant excitations corresponding to the two enhanced peaks of the solid curve in Fig. 3(b2) if $\omega_1+\omega_2-\omega_3+\omega_4\approx(\Omega_1-\Delta_{G3}/2)+\Omega_2-(\Omega_3\pm\Delta_{G4}/2)+\Omega_4$, i.e., $\Delta_3\approx\Delta_1+\Delta_2-\Delta_{G3}/2+\Delta_4\pm\Delta_{G4}/2\approx-1.5\pm 25$. Similarly, dual-enhanced peaks in Fig. 3(b3) represent two-photon resonant transitions from $|G_4\pm\rangle|G_3-\rangle$ to $|2\rangle$, respectively, if $\omega_1+\omega_2-\omega_3+\omega_4\approx(\Omega_1+\Delta_{G3}/2)+\Omega_2-(\Omega_3\pm\Delta_{G4}/2)+\Omega_4$, i.e., $\Delta_3\approx\Delta_1+\Delta_2+\Delta_{G3}/2+\Delta_4\pm\Delta_{G4}/2\approx 1.5\pm 25$. In short, dual enhancement results from the resonant pump fields while the resonance of the inner dressing field results in dual suppression.

When G_4 is small, two dips cannot be separated completely, as shown by the dashed line in Fig. 3(a). Under such

a condition, separate dressed states have not been created. Hence it is better to consider such a suppression spectrum as the result of competition between dispersion $[(\text{Re } \rho_{\text{Df1}})^2]$ and absorption $[(\text{Im } \rho_{\text{Df1}})^2]$ terms in the weak-dressing-field limit [22]. Figure 3(c) shows that, with resonant conditions ($\Delta_1=\Delta_2=0$), the DDFWM spectrum is mainly induced by the absorption term while the dispersion term is negligible [12]. By the way, we note that the spectra of Fig. 3(b1) have an absorptive shape while those of Figs. 3(b2) and (b3) have a dispersive shape due to domination of the contribution of $\text{Im } \rho_{\text{Df1}}$ in the resonant case ($\Delta_1=\Delta_2=0$) or $\text{Re } \rho_{\text{Df1}}$ in the nonresonant case ($\Delta_1+\Delta_2\neq 0$). According to Eq. (4), we have

$$(\text{Im } \rho_{\text{Df1}})^2 = (\text{Im } \rho_{f1} + \text{Im } \rho_{s1} + \text{Im } \rho_{e1})^2. \quad (11)$$

In Eq. (11), the terms $(\text{Im } \rho_{f1})^2$, $|\text{Im } \rho_{f1} \text{Im } \rho_{s1}|$, and $\text{Im } \rho_{f1} \text{Im } \rho_{e1}$ are larger than other terms by orders of magnitude. Hence we can only consider these three dominant terms. In Fig. 3(c), $(\text{Im } \rho_{f1})^2/|\rho_{f1}|^2$ is equal to 1, $\text{Im } \rho_{f1} \text{Im } \rho_{s1}$ has the negative value, and $\text{Im } \rho_{f1} \text{Im } \rho_{e1}$ has the positive value at the line center. Therefore under weak-dressing-field condition, suppression or enhancement of the FWM signal intensity is determined by destructive or constructive interferences among various MWM processes.

B. Parallel-cascade DDFWM

Next, we consider the parallel-cascade DDFWM spectra. Figures 4(a) and 4(b) show that there exist two pairs of AT splitting peaks induced by G_2 and G_4 , respectively. The positions of these peaks are determined by the intensities and the dressing field detunings. According to Eq. (5), in the limit of $|G_2|^2 \gg \Gamma_{10}\Gamma_{20}$ and $|G_4|^2 \gg \Gamma_{13}\Gamma_{14}$, we have $\Delta_{G2}=2G_2$ and $\Delta_{G4}=2G_4$. Here Δ_{G2} and Δ_{G4} are the separations induced by the two dressing fields. In fact, these two pairs of AT splitting peaks represent the transitions $|G_4\pm\rangle\rightarrow|0\rangle$ and $|0\rangle\rightarrow|G_2\pm\rangle$, as shown in Fig. 1(c2). Note that the secondarily dressed states do not exist in the parallel-cascade DDFWM.

We consider the parallel-cascade DDFWM spectra versus the dressing field detunings Δ_2 and Δ_4 as shown in Fig. 5. The FWM signal intensity without any dressing fields is normalized to be 1. Figure 5(a) shows the symmetrical suppression spectrum of the resonant FWM signal intensity ($\Delta_1=\Delta_3=0$). As the dressing fields become stronger, the suppressed dips get wider and deeper, as shown in Fig. 5(b). Figure 5(c), which has the dispersive shapes on each sides due to domination of the contribution of $\text{Re } \rho_{\text{Df2}}$, presents either suppression or enhancement of the off-resonant FWM ($\Delta_1/\Gamma_{13}=-5$) with weak dressing fields. Due to constructive superposition, the FWM signal intensity in the region ($\Delta_2/\Gamma_{13}<5, \Delta_4<4$) is the strongest. When the dressing fields get stronger, a significant enhancement of the FWM signal intensity by a factor of about 200 can be obtained in Fig. 5(d). According to dressed-state analysis and Eq. (7), the suppressed-dip conditions in Fig. 5 are $\omega_1+\omega_2=\Omega_1+\Omega_2$ (i.e., $\Delta_2=-\Delta_1$) and $\omega_1-\omega_3+\omega_4=\Omega_1-\Omega_3+\Omega_4$ (i.e., $\Delta_4=\Delta_3-\Delta_1$), respectively, while the enhanced-peak conditions are $\omega_1+\omega_2\approx(\Omega_1+\Delta_{G2}/2)+\Omega_2$ (i.e., $\Delta_2\approx-\Delta_1-\Delta_{G2}/2$) and $\omega_1-\omega_3+\omega_4\approx\Omega_1-(\Omega_3+\Delta_{G4}/2)+\Omega_4$ (i.e., $\Delta_4\approx\Delta_3-\Delta_1-\Delta_{G4}/2$), respectively.

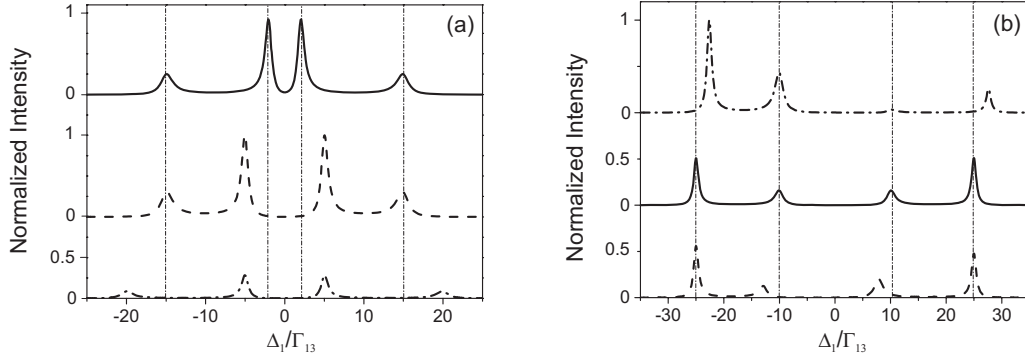


FIG. 4. Parallel-cascade DDFWM signal intensity versus Δ_1/Γ_{13} for (a) $\Delta_2=\Delta_3=\Delta_4=0$, $G_2/\Gamma_{13}=2$, $G_4/\Gamma_{13}=15$ (solid curve), $G_2/\Gamma_{13}=5$, $G_4/\Gamma_{13}=15$ (dashed curve), $G_2/\Gamma_{13}=5$, $G_4/\Gamma_{13}=20$ (dot-dashed curve); (b) $\Delta_3=0$, $G_2/\Gamma_{13}=25$, $G_4/\Gamma_{13}=10$, $\Delta_2=\Delta_4=0$ (solid curve), $\Delta_4=0$, $\Delta_2/\Gamma_{13}=-5$ (dot-dashed curve), $\Delta_2=0$, $\Delta_4/\Gamma_{13}=5$ (dashed curve). The other parameters are $\Gamma_{14}/\Gamma_{13}=0.8$, $\Gamma_{20}/\Gamma_{13}=0.5$, $\Gamma_{10}/\Gamma_{13}=0.5$. The maximum of the intensity is normalized to be 1.

C. Sequential-cascade DDFWM

Finally, we consider the sequential-cascade DDFWM spectrum. Figure 6 shows the DDFWM signal intensity versus pump field detuning Δ_3 . In Fig. 6(a), according to Eq. (7), the central peak of the solid curve is the “ $\omega_1-\omega_3$ ” two-photon resonant peak of FWM. The dashed and dot-dashed curves show that the two resonant dressing fields ($\Delta_2=\Delta_4=0$) create one pair of AT splitting peaks together. Let $\Gamma_{23}=\Gamma_{14}=\Gamma$. In the limit of $\sqrt{G_2^2+G_4^2}\gg\Gamma$, we have

$\Delta_{G_2,G_4}\approx 2\sqrt{G_2^2+G_4^2}$. Here Δ_{G_2,G_4} is separation induced by the two dressing fields together. From the dressed-state picture, there exist the common dressed states $|(G_2, G_4)\pm\rangle$ which make the “ $\omega_1-\omega_3$ ” two-photon process resonant.

Figure 6(b) depicts the primary and the secondary AT splittings by the two dressing fields, which are the same as in the nested-cascade DDFWM case (Fig. 2). The symmetrical peaks in the solid curve of Fig. 6(b) are a pair of the primary AT splitting peaks induced by the dressing field E_4 with

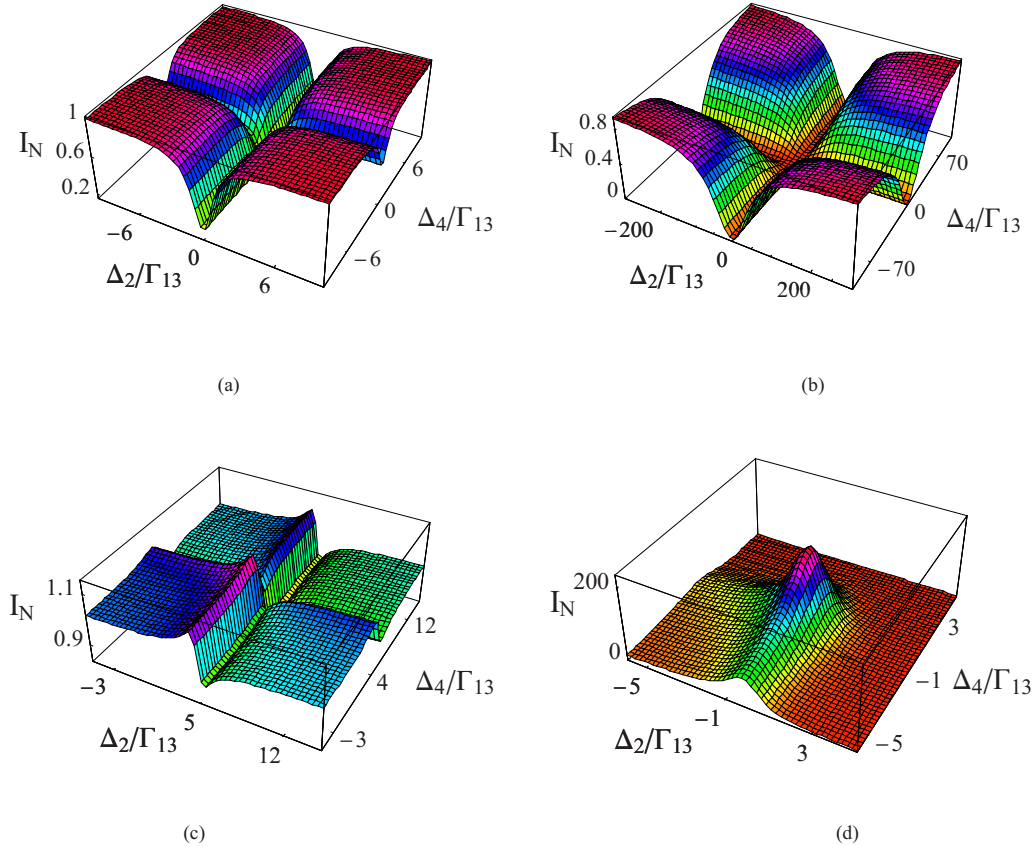


FIG. 5. (Color online) Parallel-cascade DDFWM signal intensity versus Δ_2/Γ_{13} and Δ_4/Γ_{13} for (a) $\Delta_1=\Delta_3=0$, $G_2/\Gamma_{13}=G_4/\Gamma_{13}=0.5$; (b) $\Delta_1=\Delta_3=0$, $G_2/\Gamma_{13}=G_4/\Gamma_{13}=5$; (c) $\Delta_3=0$, $\Delta_1/\Gamma_{13}=-5$, $G_2/\Gamma_{13}=G_4/\Gamma_{13}=0.5$; (d) $\Delta_3=0$, $\Delta_1/\Gamma_{13}=-5$, $G_2/\Gamma_{13}=G_4/\Gamma_{13}=5$. The other parameters are $\Gamma_{14}/\Gamma_{13}=0.8$, $\Gamma_{20}/\Gamma_{13}=0.5$, $\Gamma_{10}/\Gamma_{13}=0.5$. The FWM signal intensity with no dressing fields is normalized to be 1.

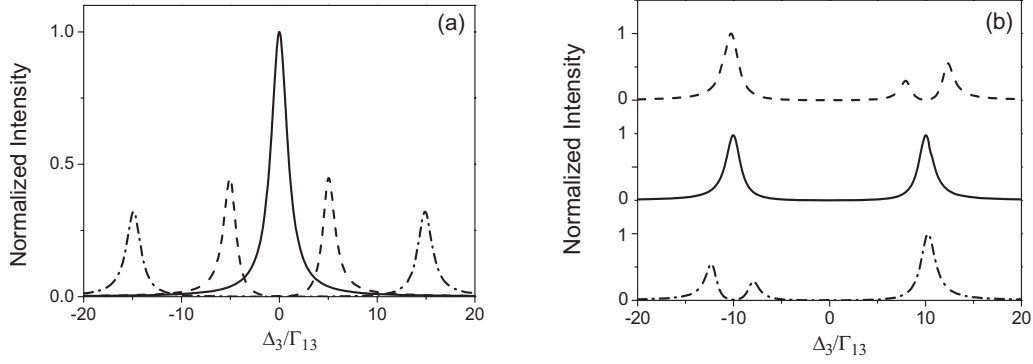


FIG. 6. Sequential-cascade DDFWM signal intensity versus Δ_3/Γ_{13} for (a) $\Delta_1=\Delta_2=\Delta_4=0$, $G_2/\Gamma_{13}=0$, $G_4/\Gamma_{13}=0$ (solid curve), $G_2/\Gamma_{13}=5$, $G_4/\Gamma_{13}=0$ (dashed curve), $G_2/\Gamma_{13}=5$, $G_4/\Gamma_{13}=14$ (dot-dashed curve); (b) $\Delta_1=\Delta_4=0$, $G_4/\Gamma_{13}=10$, $G_2/\Gamma_{13}=3$, $\Delta_2/\Gamma_{13}=1000$ (solid curve), $\Delta_2/\Gamma_{13}=10$ (dashed curve), $\Delta_2/\Gamma_{13}=-10$ (dot-dashed curve). The other parameters are $\Gamma_{23}/\Gamma_{13}=0.5$, $\Gamma_{10}/\Gamma_{13}=0.5$, $\Gamma_{14}/\Gamma_{13}=0.8$. The maximum of the intensity is normalized to be 1.

separation $\Delta_{G4} \approx 2G_4$. As $\Delta_2 \approx \pm \Delta_{G4}/2$, there exists the secondary AT splitting in the dashed or the dot-dashed curves induced by the dressing field E_2 . Similarly, the dressing field E_2 with $\Delta_2=0$ can induce the primarily dressed states while the dressing field E_4 with $\Delta_4 \approx \pm \Delta_{G2}/2$ induces the secondarily dressed states.

Then we consider the sequential-cascade DDFWM spectrum versus the dressing field detunings Δ_2 and Δ_4 . Figure

7(a) gives the symmetrically suppressed spectrum at on-resonant conditions ($\Delta_1=\Delta_3=0$). As G_2 and G_4 increase, the suppressed dips get not only wider and deeper but also asymmetrical, as shown in Fig. 7(b). Figure 7(c) shows either suppression or enhancement of the off-resonant FWM ($\Delta_3/\Gamma_{13}=5$) with weak dressing fields. Due to the constructive superposition, the FWM signal intensity in the region ($\Delta_2/\Gamma_{13} < 5$, $\Delta_4/\Gamma_{13} < 4$) is the strongest. However, under

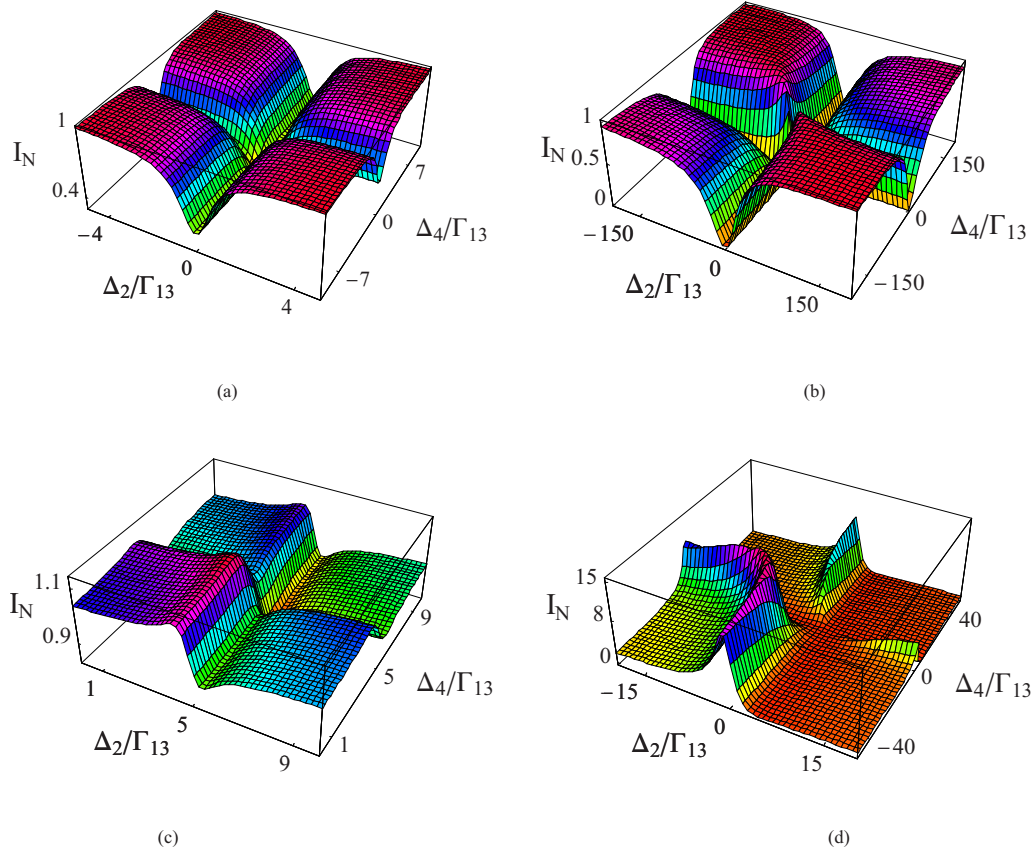


FIG. 7. (Color online) Sequential-cascade DDFWM signal intensity versus Δ_2/Γ_{13} and Δ_4/Γ_{13} for (a) $\Delta_1=\Delta_3=0$, $G_2/\Gamma_{13}=G_4/\Gamma_{13}=0.5$; (b) $\Delta_1=\Delta_3=0$, $G_2/\Gamma_{13}=G_4/\Gamma_{13}=5$; (c) $\Delta_1=0$, $\Delta_3/\Gamma_{13}=5$, $G_2/\Gamma_{13}=G_4/\Gamma_{13}=0.5$; (d) $\Delta_1=0$, $\Delta_3/\Gamma_{13}=5$, $G_2/\Gamma_{13}=G_4/\Gamma_{13}=5$. The other parameters are $\Gamma_{23}/\Gamma_{13}=0.5$, $\Gamma_{10}/\Gamma_{13}=0.5$, $\Gamma_{14}/\Gamma_{13}=0.8$. The FWM signal intensity with no dressing fields is normalized to be 1.

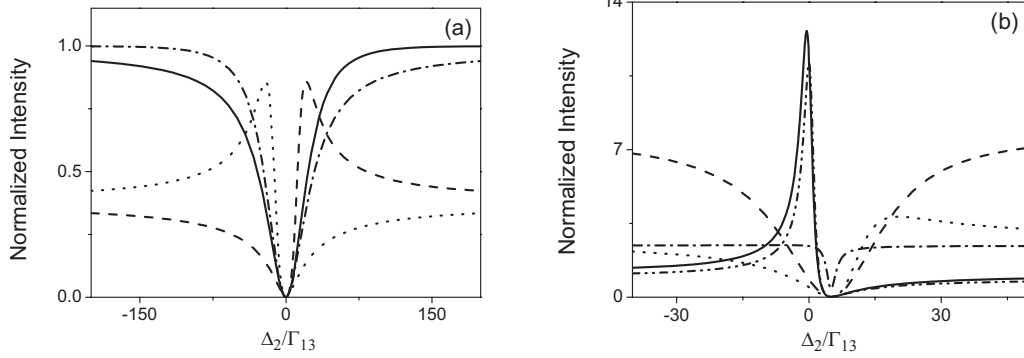


FIG. 8. (a) The cross section versus Δ_2/Γ_{13} of Fig. 7(b) for $\Delta_4/\Gamma_{13}=-200$ (solid curve), $\Delta_4/\Gamma_{13}=-20$ (dashed curve), $\Delta_4/\Gamma_{13}=20$ (dotted curve), $\Delta_4/\Gamma_{13}=200$ (dot-dashed curve); (b) the cross section versus Δ_2/Γ_{13} of Fig. 7(d) for $\Delta_4/\Gamma_{13}=-100$ (solid curve), $\Delta_4/\Gamma_{13}=100$ (dot-dot-dashed curve), $\Delta_4/\Gamma_{13}=1.5$ (dotted curve), $\Delta_4/\Gamma_{13}=0.2$ (dashed curve), $\Delta_4/\Gamma_{13}=5$ scaled by a factor of 100 (dot-dashed curve).

the condition of strong dressing fields, enhancement of only a factor of about 15 is obtained and there are no significant enhancement peaks in Fig. 7(d).

We can analyze the spectra with strong dressing fields in detail. Figure 8(a) versus Δ_2 is the cross section of Fig. 7(b). The solid and dot-dashed curves with large detuning ($\Delta_4/\Gamma_{13}=\pm 200$) are almost symmetrical. However, in the case of small detuning $\Delta_4/\Gamma_{13}=-20$ ($\Delta_4/\Gamma_{13}=20$), the dashed (dotted) curve has a peak on the right (left) side. According to Eq. (7), the DDFWM signal intensity is proportional to

$$\left(\Gamma_{13}^2 + \frac{(\Gamma_{14}^2 |G_2|^2 + \Gamma_{23}^2 |G_4|^2)^2 + (|G_2|^2 \Delta_4 + |G_4|^2 \Delta_2)^2}{(\Gamma_{14}^2 + \Delta_4^2)(\Gamma_{23}^2 + \Delta_2^2)} \right)^{-1}. \quad (12)$$

We can see that when $|G_2|^2 \Delta_4 + |G_4|^2 \Delta_2 = 0$, peaks in the dashed and dotted curves can be obtained. Hence, the asymmetry in Fig. 8(a) is induced by interaction between the two dressing fields. Such interaction weakens the suppressed effect of the single dressing field. Figure 8(b) versus Δ_2 is the cross section of Fig. 7(d). Under the condition of large detuning ($\Delta_4/\Gamma_{13}=\pm 100$) of the dressing field E_4 , the solid and dot-dot-dashed curves in Fig. 8(b) have almost similar profiles in which the suppression or enhancement of FWM signal intensity is mainly induced by the dressing field E_2 . With dressed-state analysis and Eq. (7), the suppressed dip and enhanced peak are at $\omega_1 + \omega_2 - \omega_3 = \Omega_1 + \Omega_2 - \Omega_3$ (i.e., $\Delta_2 = \Delta_3 - \Delta_1$) and $\omega_1 + \omega_2 - \omega_3 \approx (\Omega_1 + \Delta_{G2}/2) + \Omega_2 - \Omega_3$ (i.e., $\Delta_2 \approx \Delta_3 - \Delta_1 - \Delta_{G2}/2$), respectively. FWM signal intensity is enhanced by a factor of about 13. According to these two curves, we can hardly observe the constructive superposition under the strong dressing-field condition in the sequential-cascade scheme in Fig. 7(d). As Δ_4 is changed closer to $\Delta_4/\Gamma_{13}=(\Delta_3 - \Delta_1)/\Gamma_{13}=5$, the profiles of the dashed, dotted, and dot-dashed curves fluctuate violently, which shows that the interactions between the two dressing fields are strong and complex. Both the dashed and dot-dashed curves have the dip profile but the difference in height between them is quite large (the dot-dashed curve is scaled by a factor of 100). The dotted curve has a different profile from that of the

solid and the dot-dot-dashed curves (the enhanced peak is on the right of the suppressed peak).

As mentioned in Sec. II, the interaction between the two dressing fields in the nested-cascade scheme is the strongest and that of the parallel-cascade scheme is the weakest. This conclusion is verified further in the simulated spectra.

First, from the aspect of the AT splitting spectrum, the dressing fields of the nested-cascade scheme are entangled tightly with each other and have strong interaction. In Fig. 2, only the inner dressing field E_3 can create the primary AT splitting, based on which the outer dressing field E_4 can create the secondary AT splitting. On the other hand, for the parallel-cascade scheme, the dressing fields have a weaker interaction and they can directly create two independent AT splittings (Fig. 4). However, for the sequential-cascade scheme, the dressing fields can also directly create AT splitting but they have a strong interaction to create the primary and secondary AT splittings, as shown in Fig. 5(b).

Second, from the aspect of suppression or enhancement spectrum, both dressing fields E_2 and E_4 can influence the FWM signal intensity directly (Figs. 5 and 7) for the parallel- and sequential-cascade schemes, while for the nested-cascade scheme the inner dressing field E_3 suppresses or enhances FWM signal intensity directly through a pair of channels created by the outer dressing field E_4 . In the case of weak dressing fields, the interaction of the sequential-cascade scheme is negligible, and Figs. 7(a) and 7(c) are similar to Figs. 5(a) and 5(c) of the parallel-cascade DDFWM. However, with strong dressing fields the interaction gets stronger, and Figs. 7(b) and 7(d) become quite different from Figs. 5(b) and 5(d).

IV. COMPETITION BETWEEN TWO COEXISTING DRESSED MWM

We have investigated the nested-, parallel-, and sequential-cascade DDFWM processes in a five-level system interacting with seven laser fields. All the DDFWM processes, as well as DSWM processes, can coexist by carefully arranging the weak probe field E_1 and the other six coupling fields $E_2, E_2', E_3, E_3', E_4,$ and E_4' [7–9,14–17]. The interactions [mutual dressing processes and constructive (or de-

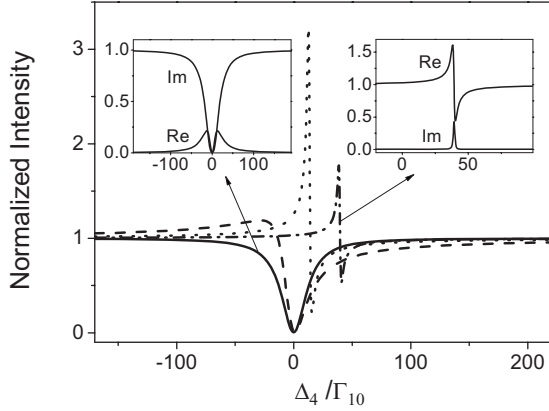


FIG. 9. DSWM signal intensity versus Δ_4/Γ_{10} for $\Delta_1=\Delta_2=0$, $G_4/\Gamma_{10}=5$, $\Delta_3=0$ (solid curve), $\Delta_3/\Gamma_{10}=1$ (dashed curve), $\Delta_3/\Gamma_{24}=15$ (dotted curve), and $\Delta_3/\Gamma_{10}=40$ (dot-dashed curve). The inset plots show comparisons of $\text{Im}=\text{Im}^2 \rho_{\text{DS1}}$ and $\text{Re}=\text{Re}^2 \rho_{\text{DS1}}$. The other parameters are $\Gamma_{20}/\Gamma_{10}=0.8$, $\Gamma_{13}/\Gamma_{10}=1$, $\Gamma_{14}/\Gamma_{10}=0.8$. The SWM signal intensity with no dressing field is normalized to be 1.

structive) interference [17]] between two different DDFWM (DSWM) processes are induced for the pump field of one DDFWM (DSWM) to be the dressing field of the other DDFWM (DSWM), and vice versa. In this section, we first study the interactions between two DSWM processes and then further investigate the interactions of two DDFWM processes that are more complicated than the former.

A. Interactions between two DSWM processes

As shown in Fig. 1(d1), in the $|3\rangle-|0\rangle-|1\rangle-|2\rangle$ subsystem the SWM process uses one photon each from E_1 , E_2 , E'_2 and two photons from E_3 . The strong-coupling field E_4 dresses such SWM process via the perturbation chain (DS1) $\rho_{00}^{(0)} \xrightarrow{\omega_1} \rho_{10}^{(1)} \xrightarrow{\omega_2} \rho_{20}^{(2)} \xrightarrow{-\omega_2} \rho_{10}^{(3)} \xrightarrow{-\omega_3} \rho_{1G4\pm}^{(4)} \xrightarrow{\omega_3} \rho_{10}^{(5)}$, and we have

$$\rho_{\text{DS1}} = \rho_{10}^{(5)} = \frac{iG_A |G_3|^2 \exp(i\mathbf{k}_{s1} \cdot \mathbf{r})}{d_1^3 d_2 (d_3 + |G_4|^2/d_6)}. \quad (13)$$

Figure 9 presents either suppression or enhancement of the SWM signal intensity versus the dressing field detuning Δ_4 . The SWM signal intensity with no dressing field is normalized to be 1 in Fig. 9. According to Eq. (13) and dressed-state analysis, the dressing field E_4 creates the dressed states $|G_4 \pm\rangle$ from $|3\rangle$ so as to impact on the “ $\omega_1 - \omega_3$ ” two-photon transition of the SWM process as shown in Fig. 1(d2). Hence, we can deduce that the suppressed dip and the enhanced peak are at $\omega_1 - \omega_3 + \omega_4 = \Omega_1 - \Omega_3 + \Omega_4$ (i.e., $\Delta_4 = \Delta_3 - \Delta_1$) and $\omega_1 - \omega_3 + \omega_4 \approx \Omega_1 - (\Omega_3 - \Delta_{G4}/2) + \Omega_4$ [i.e., $\Delta_4 \approx \Delta_3 - \Delta_1 - \Delta_{G4}/2$ as shown in Fig. 1(d2)], respectively. Also, the profile in Fig. 9 can be considered as the result of a competition between dispersion and absorption parts of DSWM [12]. At the on-resonant condition ($\Delta_1 = \Delta_2 = \Delta_3 = 0$), the value of the absorption part [$\text{Im} = (\text{Im} \rho_{\text{DS1}})^2$] is much larger than that of the dispersion part [$\text{Re} = (\text{Re} \rho_{\text{DS1}})^2$], as shown in the left inset plot of Fig. 9. Thus, the DSWM spectrum has the absorption profile (the solid curve in Fig. 9). However, for the off-resonant SWM, the value of the

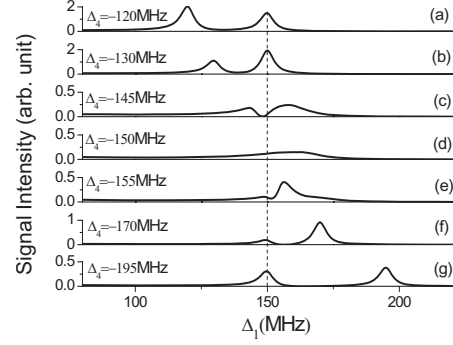


FIG. 10. The total signal intensity constituted by two DSWM ρ_{DS1} and ρ_{DS2} versus Δ_1 for the different Δ_4 values: (a) $\Delta_4 = -120$ MHz, (b) -130 MHz, (c) -145 MHz, (d) -150 MHz, (e) -155 MHz, (f) -170 MHz, and (g) -195 MHz. The other parameters are $G_2=50$ MHz, $G_3=100$ MHz, $G_4=50$ MHz, $\Delta_3=0$, and $\Delta_2=-150$ MHz.

absorption part is decreased while that of the dispersion part is increased simultaneously as shown in the right inset plot. As a result, with large detuning ($\Delta_3/\Gamma_{10}=40$), the profile of the DSWM spectrum is dominated by the dispersion part and changes to a dispersionlike profile.

Similarly, as shown in Fig. 1(d3), the other SWM process (using one photon each from E_1 , E_3 , E'_3 and two photons from E_4) is dressed by the strong-coupling field E_2 via the perturbation chain (DS2) $\rho_{00}^{(0)} \xrightarrow{\omega_1} \rho_{G2\pm 0}^{(1)} \xrightarrow{-\omega_3} \rho_{13}^{(2)} \xrightarrow{\omega_4} \rho_{14}^{(3)} \xrightarrow{-\omega_4} \rho_{13}^{(4)} \xrightarrow{\omega_3} \rho_{10}^{(5)}$, which gives

$$\rho_{\text{DS2}} = \rho_{10}^{(5)} = \frac{iG_B |G_4|^2 \exp(i\mathbf{k}_{s3} \cdot \mathbf{r})}{d_1 d_3^2 d_6 (d_1 + |G_2|^2/d_2)}. \quad (14)$$

According to Eq. (14) and the dressed-state picture in Fig. 1(d4), ρ_{DS2} is greatly suppressed at $\omega_1 + \omega_2 = \Omega_1 + \Omega_2$ (i.e., $\Delta_1 + \Delta_2 = 0$), as shown in Fig. 1(d4), or enhanced at $\omega_1 + \omega_2 \approx (\Omega_1 \pm \Delta_{G2}/2) + \Omega_2$ (i.e., $\Delta_1 + \Delta_2 \pm \Delta_{G2}/2 \approx 0$).

Note that these two DSWM processes (ρ_{DS1} and ρ_{DS2}) have an interesting relationship, i.e., the pump field E_2 of ρ_{DS1} is the dressing field of ρ_{DS2} , while the pump field E_4 of ρ_{DS2} is the dressing field of ρ_{DS1} . So these two DSWM processes dress each other. Since these two DSWM signal fields copropagate in the same direction, the total signal will be proportional to the mod square of $\rho_{\text{sum}}(\Delta)$, where $\rho_{\text{sum}}(\Delta) = \rho_{\text{DS1}} + \rho_{\text{DS2}}$ with $\Delta = \Delta_2 - \Delta_4$. Figure 10 presents evolutions of the total signal intensity versus the probe field detuning Δ_1 for different Δ_4 values. The moving peak (shifting from left to right) represents the three-photon resonant signal (satisfying $\Delta_1 - \Delta_3 + \Delta_4 = 0$) of ρ_{DS2} and the fixed peak along the dotted line represents the two-photon resonant signal ($\Delta_1 + \Delta_2 = 0$) of ρ_{DS1} . As the strong-coupling field detuning Δ_4 is changed, the moving signal of ρ_{DS2} is first greatly suppressed in Fig. 10(d) and then enhanced in Fig. 10(f) while the fixed signal of ρ_{DS1} is enhanced in Fig. 10(b) and greatly suppressed in Figs. 10(c) and 10(d). In fact, variations of the signal intensities of ρ_{DS1} and ρ_{DS2} are induced through mutual dressing processes and constructive or destructive interference as described in the following.

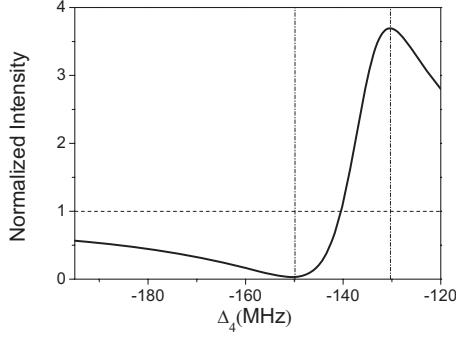


FIG. 11. The DSWM signal intensity of ρ_{Ds1} versus Δ_4 for $\Delta_1 = 150$ MHz, $\Delta_2 = -150$ MHz, $\Delta_3 = 0$, and $G_4 = 50$ MHz. The SWM signal intensity with no dressing field is normalized to be 1.

We first consider mutual dressing processes. As Δ_4 is changed, according to the dressed-state analysis, the moving peak (satisfying $\Delta_1 = \Delta_3 - \Delta_4$) of ρ_{Ds2} with the dressing field E_2 first satisfies the suppression condition $\Delta_1 = -\Delta_2$ (i.e., $\Delta_4 = \Delta_2 + \Delta_3 = -150$ MHz) and then the enhancement condition $\Delta_1 \approx -\Delta_2 + \Delta_{G2}/2$ (i.e., $\Delta_4 \approx \Delta_2 + \Delta_3 - \Delta_{G2}/2 \approx -170$ MHz) while the fixed peak (satisfying $\Delta_1 = -\Delta_2$) of ρ_{Ds1} with the dressing field E_4 first satisfies the enhancement condition ($\Delta_1 \approx \Delta_3 - \Delta_4 + \Delta_{G4}/2$, i.e., $\Delta_4 \approx \Delta_2 + \Delta_3 + \Delta_{G4}/2 \approx -130$ MHz) and then the suppression condition ($\Delta_1 = \Delta_3 - \Delta_4$, i.e., $\Delta_4 = \Delta_2 + \Delta_3 = -150$ MHz). Figure 11 shows the fixed signal intensity of ρ_{Ds1} versus Δ_4 . Here the SWM signal intensity with no dressing field ($G_4 = 0$) is normalized to be 1. The enhanced peak and suppressed dip are located at $\Delta_4 = -130$ and -150 MHz respectively, which fit well with the evolution curve of Fig. 10.

Then we study destructive or constructive interference in this system. Based on the analysis of mutual dressing processes, we can see that when two peaks overlap with each other, the total signal intensity shows a significant suppression as shown in Fig. 10(d). However, the maximal suppression of the fixed signal occurs at about $\Delta_1 = 150$ MHz in Fig. 10(c). This is a result of destructive interference between ρ_{Ds1} and ρ_{Ds2} . In fact, constructive and destructive interferences can be converted into each other as the two peaks are tuned to overlap or separate in Fig. 10.

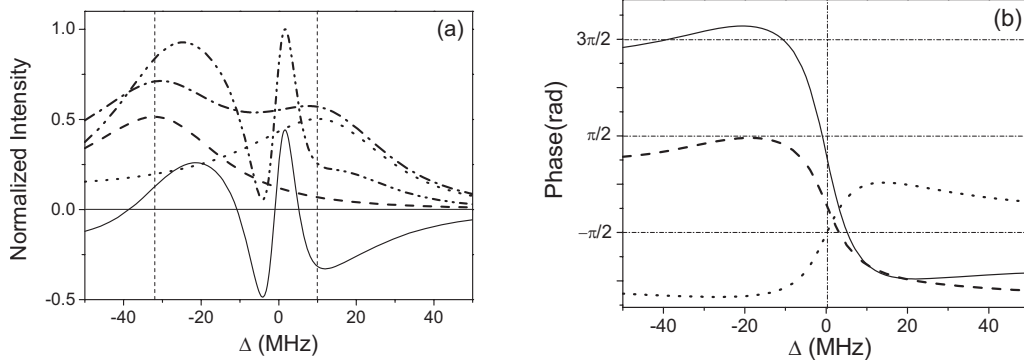


FIG. 12. (a) The total signal intensity of $|\rho_{sum}|^2$ (dot-dot-dashed curve), $|\rho_{Ds1}|^2$ (dashed curve), $|\rho_{Ds2}|^2$ (dotted curve), $|\rho_{Ds1}|^2 + |\rho_{Ds2}|^2$ (dot-dashed curve), and the interference item $2|\rho_{Ds1}||\rho_{Ds2}|\cos\theta$ (solid curve) versus Δ . Here $\Delta = \Delta_2 - \Delta_4$, $\theta = \theta_{Ds1} - \theta_{Ds2}$. The parameters are $\Delta_2 = -150$ MHz, $\Delta_3 = 0$, $\Delta_1 = -(\Delta_2 + \Delta_4)/2$, $G_2 = 50$ MHz, $G_3 = 100$ MHz, and $G_4 = 50$ MHz. The maximum intensity is normalized to 1. (b) θ_{Ds1} (dashed curve), θ_{Ds2} (dotted curve), and θ (solid curve) versus Δ .

Figure 12(a) shows the values of $|\rho_{Ds1}|^2$, $|\rho_{Ds2}|^2$, $|\rho_{Ds1}|^2 + |\rho_{Ds2}|^2$, $|\rho_{sum}|^2$, and $|\rho_{sum}|^2 - |\rho_{Ds1}|^2 - |\rho_{Ds2}|^2$ at $\Delta_1 = -(\Delta_2 + \Delta_4)/2$ (the position is between the two peaks in Fig. 10) versus the detuning difference Δ between Δ_2 and Δ_4 , respectively. $|\rho_{Ds1}|^2$ and $|\rho_{Ds2}|^2$ have the maximal values at $\Delta = -32$ MHz (dashed curve) and 10 MHz (dotted curve), respectively. Hence, there exist two peaks at around $\Delta = -32$ and 10 MHz in the dot-dashed curve that represents the value of the sum $|\rho_{Ds1}|^2 + |\rho_{Ds2}|^2$. However, with interference terms, the total signal intensity $|\rho_{sum}|^2$ has two peaks and one deep hole at $\Delta = -24$, 1.8, and -4 MHz, respectively, in the dot-dot-dashed curve. This means that the interference has a significant impact on the total signal intensity. The solid curve shows the value of the interference term, which is equal to $|\rho_{sum}|^2 - |\rho_{Ds1}|^2 - |\rho_{Ds2}|^2$. Here the value below or above zero means destructive or constructive interference. There are two constructive peaks and two destructive holes, whose amplitudes are comparable to that of both DSWM signals.

In fact, variations of phase difference between two DSWM processes change constructive interference into destructive interference, and vice versa. More specifically, letting $\rho_{Ds1} = |\rho_{Ds1}|\exp(i\theta_1)$ and $\rho_{Ds2} = |\rho_{Ds2}|\exp(i\theta_2)$, we have $|\rho_{sum}|^2 - (|\rho_{Ds1}|^2 + |\rho_{Ds2}|^2) = 2|\rho_{Ds1}||\rho_{Ds2}|\cos\theta$. Here, $\theta = \theta_1 - \theta_2$. Figure 12(b) shows the phases θ_1 (the dashed curve), θ_2 (the dotted curve), and the phase difference θ (the solid curve) versus Δ . As θ_1 and θ_2 are changed, θ alternates between 2π and $-\pi$, and the interference switches from constructive, destructive, partly constructive, and partly destructive (as given in Table I).

B. Interactions between two DDFWM processes

Since the interference effect between two DDFWM processes is similar to that of the two DSWM ones but the contribution can be one order of magnitude smaller than the mutual dressing effect, in this section we will only consider the mutual dressing processes between the nested- and parallel-cascade DDFWM.

Figure 13 shows evolutions of the total signal intensity between the nested-cascade DDFWM ρ_{Df4} in the system [Fig. 1(b1)] and the parallel-cascade DDFWM ρ_{Df5} in the

TABLE I. Evolution of θ , the constructive and the destructive interference versus Δ .

Δ	$[-50, -38.6]$	$(-38.6, -10.7]$	$(-10.7, -1]$	$(-1, 5]$	$(5, 50]$
θ	$[7\pi/5, 3\pi/2]$	$[3\pi/2, 8\pi/5]$	$[\pi/2, 3\pi/2]$	$[-\pi/2, \pi/2]$	$[-\pi/2, -\pi]$
interference	destructive	constructive	destructive	constructive	destructive

system [Fig. 1(c1)] versus the probe field detuning Δ_1 for different Δ_3 values. Here

$$\rho_{Df4} = \frac{-iG_A \exp(i\mathbf{k}_{f1} \cdot \mathbf{r})}{d_1 d_2 \left(d_1 + \frac{|G_3|^2}{d_3 + |G_4|^2/d_6} \right)}, \quad (15)$$

$$\rho_{Df5} = \frac{-iG_B \exp(i\mathbf{k}_{f2} \cdot \mathbf{r})}{d_3(d_1 + |G_2|^2/d_2)(d_7 + |G_4|^2/d_8)}. \quad (16)$$

Note that the pump field E_3 in ρ_{Df5} is the dressing field of ρ_{Df4} , while the pump field E_2 in ρ_{Df4} is the dressing field of ρ_{Df5} . So, these two DDFWM processes dress each other in this system. From Fig. 13(a) to Fig. 13(c), the right peak is the two-photon resonant ($\Delta_1 + \Delta_2 = 0$) signal of ρ_{Df4} and the left peak is the two-photon resonant ($\Delta_1 - \Delta_3 = 0$) signal of ρ_{Df5} . As Δ_3 is increased, the moving peak of ρ_{Df5} is sup-

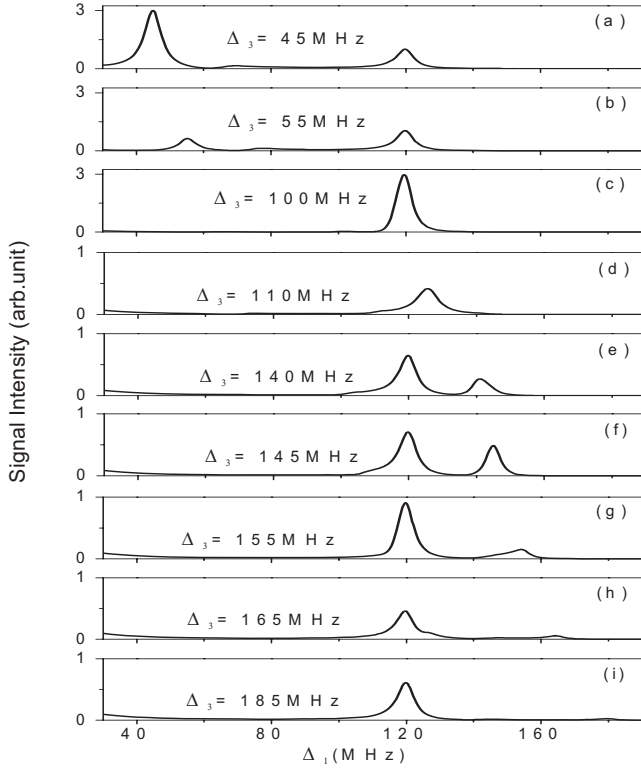


FIG. 13. The total signal intensity constituted by two DDFWM ρ_{Df4} and ρ_{Df5} versus Δ_1 for the different Δ_3 values: (a) $\Delta_3 = 45$ MHz, (b) 55 MHz, (c) 100 MHz, (d) 110 MHz, (e) 140 MHz, (f) 145 MHz, (g) 155 MHz, (h) 165 MHz, and (i) 185 MHz. The other parameters are $G_2 = 60$ MHz, $G_3 = 30$ MHz, $G_4 = 20$ MHz, $\Delta_2 = -120$ MHz, and $\Delta_4 = 30$ MHz.

pressed while the fixed peak of ρ_{Df4} is enhanced. In Fig. 13(d), as Δ_3 is increased continuously, the peak of ρ_{Df5} changes too small to be seen and the peak of ρ_{Df4} is also suppressed. From Fig. 13(e) to Fig. 13(g), the peak of ρ_{Df5} moves to the right and is enhanced at $\Delta_3 = 145$ MHz, while the fixed peak of ρ_{Df4} is enhanced again at $\Delta_3 = 155$ MHz. Finally, in Figs. 13(h) and 13(i), the fixed peak of ρ_{Df4} is suppressed again at $\Delta_3 = 165$ MHz, while the moving peak of ρ_{Df5} gets small owing to large detuning Δ_3 .

In Fig. 13, the fixed peak of ρ_{Df4} is doubly enhanced in Figs. 13(c) and 13(g) and doubly suppressed in Figs. 13(d) and 13(h). According to dressed-state analysis of the nested-cascade scheme, the dual-suppression (or dual-enhancement) results from the double resonance of the dressing field E_3 (or the probe field E_1). As the peak of ρ_{Df5} moves to the right (Δ_3 is changed), the fixed peak of ρ_{Df4} can satisfy the dual-suppression condition $\Delta_3 \approx \Delta_1 + \Delta_4 \pm \Delta_{G4}/2 \approx 110$ or 165 MHz and the dual-enhancement condition $\Delta_3 \approx \Delta_1 + \Delta_4 \pm \Delta_{G4}/2 - \Delta_{G3}/2 \approx 100$ or 155 MHz. Figure 14 plots the signal intensity of ρ_{Df4} versus Δ_3 . The FWM signal intensity with no dressing fields is normalized to be 1. The pair of suppressed or enhanced channels in Fig. 14 agree well with the evolutions shown in Fig. 13. The two enhanced peaks are located at $\Delta_3 = 100$ and 155 MHz, respectively, while the two suppressed dips are located at $\Delta_3 = 110$ and 165 MHz, respectively. Similarly, according to dressed-state analysis of the parallel-cascade scheme, the moving peak (located at $\Delta_1 = \Delta_3$) of ρ_{Df5} first satisfies the suppression condition $\Delta_1 = -\Delta_2$ (i.e., $\Delta_3 = -\Delta_2 = 120$ MHz) and then the enhancement condition $\Delta_1 \approx -\Delta_2 + \Delta_{G2}/2$ (i.e., $\Delta_3 \approx -\Delta_2 + \Delta_{G2}/2 \approx 145$ MHz).

It is important to understand the competitions (mutual-dressing processes and constructive or destructive interferences) between two coexisting MWM processes. The reso-

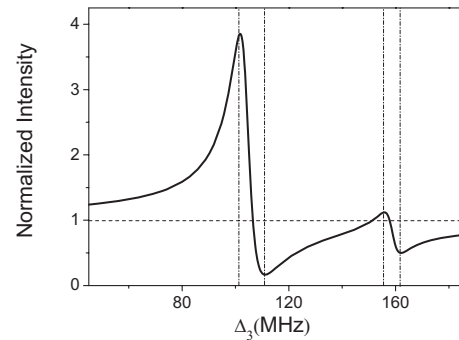


FIG. 14. The DDFWM signal intensity of ρ_{Df4} versus Δ_3 for $\Delta_1 = 120$ MHz, $\Delta_2 = -120$ MHz, $\Delta_4 = 30$ MHz, $G_2 = 60$ MHz, $G_3 = 30$ MHz, and $G_4 = 20$ MHz. The FWM signal intensity with no dressing field is normalized to be 1.

nances of the dressing field and that of the pump (probe) fields result in suppression or enhancement of MWM signal intensity. Constructive or destructive interference also has a significant influence on the total signal intensity. Through adjusting frequency detunings of the strong-coupling fields, two dressed MWM signals can be tuned together or separated, modify (suppress and enhance) each other, and affect the total signal intensity. Investigations of such interaction processes will help us to understand and optimize the generated multichannel nonlinear optical signals. One potential application of generating efficient MWM in multistate systems is to design efficient multiqubit phase gates for quantum-information processing.

V. CONCLUSION

In conclusion, we have investigated DDFWM processes in the nested-cascade, sequential-cascade, and parallel-cascade schemes theoretically in an open multidressed five-level atomic system. The interaction between the two dressing fields is the strongest in the nested-cascade scheme is the strongest but is the weakest in the parallel-cascade scheme. The sequential-cascade scheme is an intermediate case between them and shares certain common features of the other two schemes under the weak dressing field limit. There are also coexisting DSWM and EWM processes in such an open system. We have also considered competitions and interactions between coexisting nested-cascade DDFWM and

parallel-cascade DDFWM or two DSWM processes that include two physical processes, i.e., mutual-dressing processes and constructive or destructive interferences. Based on the dressed-state analysis, the resonances of the dressing field and the pump field result in suppression and enhancement of the MWM signal intensity. Constructive or destructive interference also has a significant influence on the total signal intensity for DDFWM. Investigations of those different doubly dressing schemes and interactions between various MWM processes in multilevel atomic systems can help us to understand the underlying physical mechanisms and to effectively optimize the generated multichannel nonlinear optical signals. Controlling these interaction processes can have important applications in designing novel nonlinear optical devices in multistate systems.

ACKNOWLEDGMENTS

This work was supported by the National Natural Science Foundation of China (Grants No. 60308002 and No. 60678005), the Foundation for the Author of National Excellent Doctoral Dissertation of China (Grant No. 200339), the Foundation for the Key Program of the Ministry of Education, China (Grant No. 105156), the For Ying-Tong Education Foundation for Young Teachers in the Institutions of Higher Education of China (Grant No. 101061), and the Specialized Research Fund for the Doctoral Program of Higher Education of China (Grant No. 20050698017).

-
- [1] P. R. Hemmer, D. P. Katz, J. Donoghue, M. Cronin-Golomb, M. S. Shahriar, and P. Kumar, *Opt. Lett.* **20**, 982 (1995).
 - [2] Y. Li and M. Xiao, *Opt. Lett.* **21**, 1064 (1996); B. Lu, W. H. Burkett, and M. Xiao, *ibid.* **23**, 804 (1998).
 - [3] Y. V. Rostovtsev, Z. E. Sariyanni, and M. O. Scully, *Phys. Rev. Lett.* **97**, 113001 (2006).
 - [4] D. A. Braje, V. Balic, S. Goda, G. Y. Yin, and S. E. Harris, *Phys. Rev. Lett.* **93**, 183601 (2004).
 - [5] H. Kang, G. Hernandez, and Y. F. Zhu, *Phys. Rev. Lett.* **93**, 073601 (2004).
 - [6] Z. C. Zuo, J. Sun, X. Liu, Q. Jiang, S. G. Fu, L. A. Wu, and P. M. Fu, *Phys. Rev. Lett.* **97**, 193904 (2006).
 - [7] Y. P. Zhang, A. W. Brown, and M. Xiao, *Opt. Lett.* **32**, 1120 (2007).
 - [8] Y. P. Zhang and M. Xiao, *Appl. Phys. Lett.* **90**, 111104 (2007).
 - [9] Y. P. Zhang, A. W. Brown, and M. Xiao, *Phys. Rev. Lett.* **99**, 123603 (2007).
 - [10] M. D. Lukin, S. F. Yelin, M. Fleischhauer, and M. O. Scully, *Phys. Rev. A* **60**, 3225 (1999).
 - [11] M. Yan, E. G. Rickey, and Y. F. Zhu, *Phys. Rev. A* **64**, 013412 (2001).
 - [12] A. Joshi and M. Xiao, *Phys. Rev. A* **72**, 062319 (2005).
 - [13] A. Joshi and M. Xiao, *Phys. Rev. A* **71**, 041801 (2005).
 - [14] Y. P. Zhang, A. W. Brown, C. L. Gan, and M. Xiao, *J. Phys. B* **40**, 3319 (2007).
 - [15] Y. P. Zhang and M. Xiao, *Opt. Express* **15**, 7182 (2007).
 - [16] Y. P. Zhang, B. Anderson, and M. Xiao, *J. Phys. B* **41**, 045502 (2008).
 - [17] Y. P. Zhang, B. Anderson, A. W. Brown, and M. Xiao, *Appl. Phys. Lett.* **91**, 061113 (2007).
 - [18] S. W. Du, J. M. Wen, M. H. Rubin, and G. Y. Yin, *Phys. Rev. Lett.* **98**, 053601 (2007); S. W. Du, Eun Oh, J. M. Wen, and M. H. Rubin, *Phys. Rev. A* **76**, 013803 (2007).
 - [19] Y. Wu and L. Deng, *Phys. Rev. Lett.* **93**, 143904 (2004).
 - [20] Y. Wu, J. Saldana, and Y. F. Zhu, *Phys. Rev. A* **67**, 013811 (2003).
 - [21] D. J. Ulness, J. C. Kirkwood, and A. C. Albrecht, *J. Chem. Phys.* **108**, 3897 (1998); K. D. Moll, D. Homoelle, A. L. Gaeta, and R. W. Boyd, *Phys. Rev. Lett.* **88**, 153901 (2002).
 - [22] S. E. Harris, *Phys. Today* **50**(7), 36 (1997); J. Gea-Banacloche, Y. Li, S. Jin, and M. Xiao, *Phys. Rev. A* **51**, 576 (1995).